




**Steering of circular dichroism in biharmonic ionization of atoms**A. V. Volotka <sup>1,2,3</sup>, J. Hofbrucker <sup>1,2</sup> and S. Fritzsche <sup>1,2,4</sup><sup>1</sup>*Helmholtz-Institut Jena, Fröbelstieg 3, D-07743 Jena, Germany*<sup>2</sup>*GSI Helmholtzzentrum für Schwerionenforschung GmbH, Planckstrasse 1, D-64291 Darmstadt, Germany*<sup>3</sup>*Department of Physics and Engineering, ITMO University, Kronverskiy Prospekt 49, 197101 Saint Petersburg, Russia*<sup>4</sup>*Theoretisch-Physikalisches Institut, Friedrich-Schiller-Universität Jena, Max-Wien-Platz 1, D-07743 Jena, Germany*

(Received 13 November 2020; accepted 27 August 2021; published 22 September 2021)

Circular dichroism in photoelectron angular distributions of general biharmonic (i.e.,  $n\omega + m\omega$ ) atomic ionization is analyzed theoretically and given along with “experimental guidelines” on how it can be steered towards its maximum. It is shown that such a maximum circular dichroism can always be achieved for the ionization of an arbitrary atom and for any incident fundamental photon energy by fine control of only two experimental parameters: the relative flux and phase difference of the two components of the radiation field. In this Letter, we provide a simple analytical description of the circular dichroism as well as a set of rules which enables full control over its magnitude. Our findings are demonstrated explicitly for the ionization of helium with a two-color field composing a fundamental beam and its second harmonic.

DOI: [10.1103/PhysRevA.104.L031103](https://doi.org/10.1103/PhysRevA.104.L031103)

Circular dichroism in atomic photoionization is known to be nonzero only if the atoms are initially polarized or if the photoelectron spin orientation is detected [1,2]. This holds true for one-, two-, or generally multiphoton ionization by monochromatic light [3]. However, for atoms irradiated by a two-color field, dependence on the helicity of the two beam components may arise. Dichroic phenomena in two-color multiphoton ionization of atoms have therefore attracted a great deal of experimental as well as theoretical attention. Typical dichroism measurements comprise an atomic target ionized by a beam consisting of circularly polarized extreme ultraviolet (XUV) and either co- or counterrotating infrared (IR) pulses [4–12]. The circular dichroism for such pump-probe experiments refers to the change in the helicity of the IR pulse and vanishes if the helicities of both IR and XUV are reversed. The origin of the circular dichroism has a straightforward physical explanation. The XUV pulse pumps the atomic system with a well-defined projection of angular momentum, while the IR beam subsequently already interacts with an already polarized target, which leads to dichroic behavior.

In this work, we consider a different kind of circular dichroism, one which remains after reversing the handedness of all particles in the initial state. Particularly, we investigate the ionization of atoms by circularly polarized *biharmonic beams*, i.e., two-color copropagating beams consisting of two commensurable  $n\omega + m\omega$  frequencies. Atoms exposed to such biharmonic fields undergo  $n$ -photon (with  $m\omega$ ) and  $m$ -photon (with  $n\omega$ ) ionization, where both ionization processes lead to final photoelectron states with identical energy [13,14]. Figure 1 shows a schematic representation of the process, together with co- and counterrotating examples of electric fields of biharmonic beams. In strong contrast to the two-color (XUV + IR) ionization, the circular dichroism in biharmonic

ionization has a fundamentally different origin. Rather than arising from the prior polarization (of the magnetic substate) of the target, the circular dichroism in biharmonic ionization has a pure *interference* nature. Actually, neither of the ( $n$ - or  $m$ -photon) ionization processes alone causes dichroic behavior, but the interference between the two ionization pathways leads to photoelectron angular distributions, which are sensitive to the handedness of the light field.

Biharmonic ionization of atoms has been dominantly investigated in the so-called strong-field regime at optical or infrared photon wavelengths [15–20]. In this low-frequency interaction regime, the interaction of atoms with biharmonic fields was applied to create and control, for example, electron vortices [21–23] or to generate circularly polarized high-harmonic fields [24]. At free-electron laser facilities, the generation of biharmonic beams with XUV energies became possible only recently and triggered both theoretical [25–27] and experimental [28–30] efforts. In contrast to the low-frequency regime, the ionization of atoms with biharmonic XUV beams allows one to study the interaction from a different perspective, where the atomic Coulomb field dominates over the light field. The first pioneering experiments [28–30] performed the ionization of helium and neon atoms by fundamental frequency and its second harmonic. These experiments demonstrated that the photoelectron angular distribution can be controlled by variation of the relative phase between the two beam components and their relative flux. Here, we show that the circular dichroism in the photoelectron angular distribution from the  $n \oplus m$ -photon biharmonic below-threshold ionization of  $s$  electrons can be fully controlled by just two experimental parameters (Fig. 1). Moreover, we demonstrate that maximum circular dichroism  $\Delta_{\text{CD}} = \pm 1$  can be obtained for biharmonic ionization of any atom independent of the choice of the fundamental photon frequency.

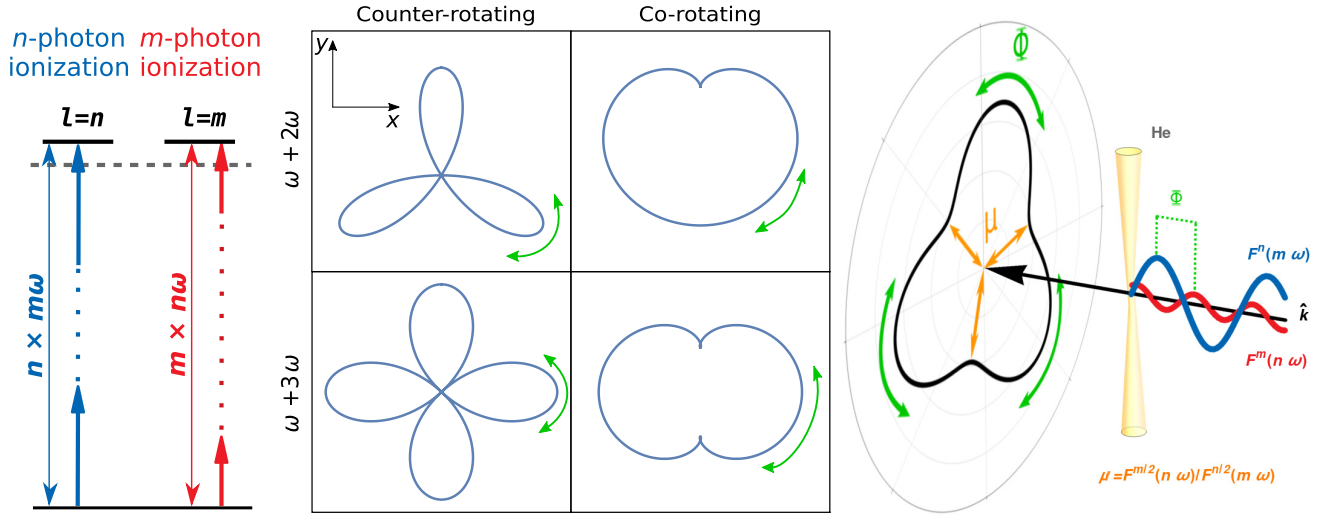


FIG. 1. Schematic representation of biharmonic ionization of atoms. Left: Energy scheme for the ionization of atoms by a circularly polarized  $m\omega + n\omega$  biharmonic beam which leads to  $n$ - and  $m$ -photon ionization. The photoelectron wave function consists of the individual contributions of the two processes as well as their interference. Middle: Electric fields of biharmonic beams that consist of a fundamental frequency and its second (top) or third (bottom) harmonic. The shape of the electric field also depends on whether the two components are counter- (left) or corotating (right). Right: Sketch of the biharmonic ionization process. Just two experimental parameters (relative flux  $\mu$  and phase  $\Phi$  between the two colors of the field) are sufficient to control the circular dichroism. Their effect on an example photoelectron angular distribution is shown.

The electric field of circularly polarized biharmonic light beams consists of two copropagating co- or counterrotating circularly polarized components with frequencies which are integer multiples ( $n$  and  $m$ ) of a fundamental frequency  $\omega$ . This electric field can be written as

$$E(t) = \frac{i}{2} (E_n \epsilon_{\lambda_n} e^{-in\omega t} + E_m \epsilon_{\lambda_m} e^{-im\omega t + i\Phi}) + \text{c.c.}, \quad (1)$$

where the amplitude of the electric field of each component is represented by  $E_{n,m}$  and the phase shift between them is represented by  $\Phi$ . This (phase) shift determines the orientation of maxima of the electric field within the polarization plane, while the rotation direction of the electric field of each component is given by its helicity  $\lambda_{n,m}$ . The middle plot of Fig. 1 shows four examples of the electric field of biharmonic beams with different harmonic orders and polarization states. The top row shows the electric field for a beam consisting of a fundamental frequency and its second harmonic ( $\omega + 2\omega$ ), while the bottom row shows a beam of fundamental frequency and its third harmonic ( $\omega + 3\omega$ ). Beams of both counterrotating (left) and corotating (right) components are presented.

As seen from Fig. 1, the interaction of atoms with fields of  $n\omega$  and  $m\omega$  frequencies will, accordingly, lead to  $m$ - and  $n$ -photon ionizations. More generally, *additional* ionization pathways arise if  $n$  and  $m$  share a common divider due to the absorption of photons from both beam components. However, we will restrict our analysis to the case where  $n$  and  $m$  have no common divider and the ionization process proceeds only through  $n$ - or  $m$ -photon ionization pathways. Furthermore, it was shown before [30–32] that ionization of atoms by long pulses, as they are often produced by the current free-electron laser facilities, can be well described by assumption of infinitely long pulses. Since we focus on ionization at such facilities, we will adopt the long-pulse approximation.

Biharmonic  $n$ - and  $m$ -photon ionizations of  $s$  electrons by circularly polarized light lead to the angular part of the photoelectron wave function with only two dominant nonrelativistic partial waves, given by

$$\psi_{\lambda_m \lambda_n}^{nm}(\theta, \phi) = c_{nm}(\lambda_m) Y_{n, \lambda_m n} + c_{mn}(\lambda_n) e^{i\Phi} Y_{m, \lambda_n m}. \quad (2)$$

The angular dependence of this wave function is determined by two spherical harmonics,  $Y_{l, \pm l} = Y_{l, \pm l}(\theta, \phi)$ , in terms of the polar and azimuthal angles  $\theta$  and  $\phi$ , with the angular momentum directly determined by the order of the two ionization processes as well as the helicities of the incident beam components. The magnitude of each partial wave is given by the amplitudes  $c_{nm}$  ( $c_{mn}$ ), which take the form

$$c_{nm}(\lambda_m) = \frac{\sqrt{4\pi} (-2\lambda_m)^n n!}{(2n+1)!} \left( \frac{-9\pi \alpha F(m\omega)}{n\omega} \right)^{n/2} e^{i\delta_n} U_n, \quad (3)$$

where  $\delta_n$  is the partial-wave phase of the photoelectron and  $F(m\omega) = E_m^2/(m\omega)$  is the flux of the beam and the intensity  $I(m\omega) = m\omega F(m\omega)$ . Moreover, we consider here below-threshold ionization so that  $(n-1)\omega < E_b$  and  $(m-1)\omega < E_b$ , with  $E_b$  being the electron binding energy. To minimize the number of parameters needed to describe biharmonic ionization, we introduce a relative flux parameter  $\mu = \sqrt{F^m(n\omega)/F^n(m\omega)}$  with units of  $(L^{-2}T^{-1})^{(m-n)/2}$ , which enables us to obtain the photoelectron angular distributions of the ionization process without having to set specific intensities of the beam components explicitly. Each of the  $n$ th- or  $m$ th-order ionization processes proceeds through a single nonrelativistic ionization pathway. For  $n$ -photon ionization, the corresponding radial transition amplitudes  $U_n$  can be found explicitly, for example, in Ref. [33]. The expression of the angle-differential rate of biharmonic ( $n$ - and  $m$ -photon) ionization can be simply obtained from the square of the wave

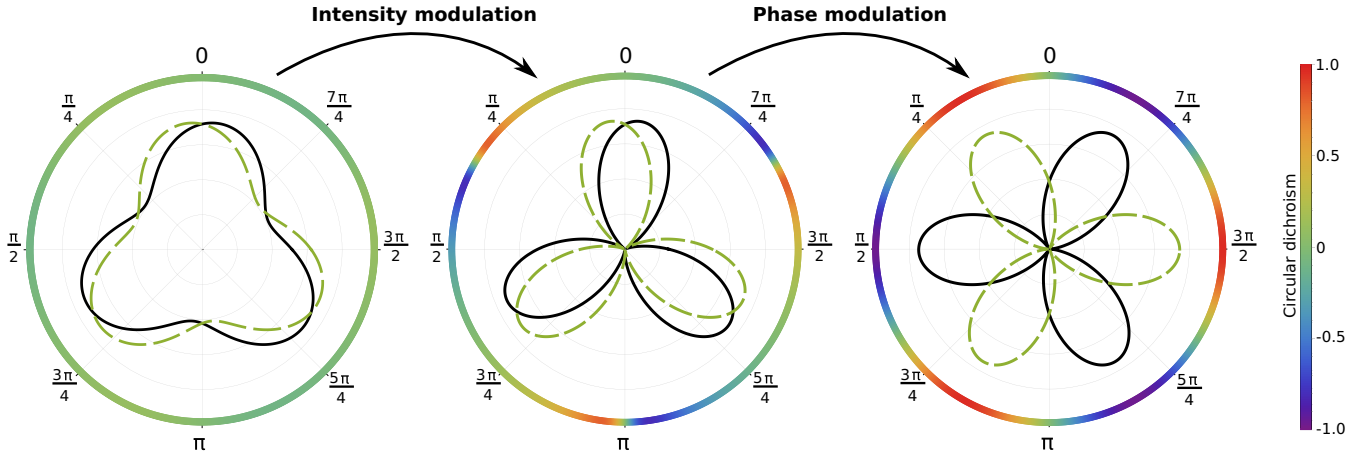


FIG. 2. Steering of circular dichroism in photoelectron angular distributions of biharmonic ionization. Ionization of helium by a counterrotating circularly polarized beam consisting of fundamental frequency and its second harmonic was chosen in order to demonstrate how the maximum circular dichroism (color-coded ring around the curves) can be obtained experimentally. Transition rates  $dW_{-1}^{12}$  (solid black line) and  $dW_{-1}^{21}$  (dashed green line) were calculated using  $\omega = 14.3$  eV. The dichroism is given by the normalized difference of these rates at particular relative flux  $\mu$  and phase difference  $\Phi$ . The leftmost plot shows photoelectron angular distributions as generally expected in biharmonic ionization measurements [using  $\mu = 2000$  natural units (n.u.) and  $\Phi = \pi/3$ ]. The distributions and circular dichroism, shown in the middle plot, are obtained if the relative flux is chosen to be  $\mu = 11\,000$  n.u. If the phase difference between the beam components is tuned to its optimal value  $\Phi = 11\pi/15$ , the distributions are rotated with respect to each other and give rise to the rightmost plot, where the maximum possible circular dichroism can be measured in six directions. The total ionization yields associated with these plots are  $W = 3.6 \times 10^{12}$  s $^{-1}$  for the left plot and  $W = 6.2 \times 10^{12}$  s $^{-1}$  for the middle and right ones.

function (2),

$$\begin{aligned}
 dW_{\lambda_m \lambda_n}^{nm} &\equiv \frac{dW_{\lambda_m \lambda_n}^{nm}}{d\Omega} = |\psi_{\lambda_m \lambda_n}^{nm}(\theta, \phi)|^2 \\
 &= F^n(m\omega) |U_n|^2 \left\{ \frac{\zeta^n}{(m\omega)^n} + \frac{\mu^2 \zeta^m |U_m/U_n|^2}{(n\omega)^m} \right. \\
 &\quad + \frac{2\mu \zeta^{(n+m)/2}}{(n\omega)^{m/2} (m\omega)^{n/2}} \text{Re}[U_m/U_n (\lambda_m)^n (\lambda_n)^m \\
 &\quad \left. \times i^{(n\lambda_m - m\lambda_n)} e^{i(\delta_m - \delta_n)} e^{i(m\lambda_n - n\lambda_m)\phi} e^{-i\Phi}] \right\}, \quad (4)
 \end{aligned}$$

where  $\zeta = 9\pi\alpha \sin^2 \theta$ . From expression (1), we can easily deduce the rotational symmetry of the electric field, which is subsequently imprinted in the photoelectron angular distribution (4) [18,34]. The distributions in the polarization plane will possess  $|n\lambda_m - m\lambda_n|$  “lobes” and hence also express  $(|n\lambda_m - m\lambda_n|)$ -fold rotational symmetry in this plane.

Expression (4) can be readily used to obtain the circular dichroism in the photoelectron angular distributions. The dichroism is defined at a particular angle as the normalized difference of the ionization rates with opposite helicities ( $dW_{\lambda_m \lambda_n}^{nm}$  and  $dW_{-\lambda_m -\lambda_n}^{nm}$ )

$$\Delta_{\text{CD}} = \frac{dW_{\lambda_m \lambda_n}^{nm} - dW_{-\lambda_m -\lambda_n}^{nm}}{dW_{\lambda_m \lambda_n}^{nm} + dW_{-\lambda_m -\lambda_n}^{nm}} \quad (5)$$

and takes values in the range  $-1 \leq \Delta_{\text{CD}} \leq 1$ . Here, we aim to find the conditions for the experimental parameters of relative flux and phase of the biharmonic beam components which ensure the maximum circular dichroism  $\Delta_{\text{CD}} = \pm 1$ .

All (atomic) interaction processes are characterized by a set of (complex) amplitudes, including real values and phases.

For biharmonic ionization of  $s$  electrons, the photoelectron angular distribution can be fully described by the amplitude ratio  $U_m/U_n$ , the difference in partial wave phases  $\delta_m - \delta_n$ , and the relative flux  $\mu$  and phase  $\Phi$  of the two beam components [see Eq. (4)]. While the former two are “atomic” properties, the latter two are determined by the experimental setup. It has been demonstrated that both experimental parameters can be controlled [28–30]. From expression (4), moreover, it can be seen that the flux ratio enters in the same power as the amplitude ratio  $U_m/U_n$ . Similarly, the phase difference between the beam components appears only in the interference term and in the same way as the phases of the partial waves of the photoelectron. By varying the relative flux  $\mu$  and phase  $\Phi$  between the two beam components, one can effectively control the contributions of the transition amplitudes as well as the phase of the ionization process and hence gain complete control over the photoelectron angular distributions. The right side of Fig. 1 displays the *control* of photoelectron angular distribution in the polarization plane. For instance, a change in the flux ratio  $\mu$  affects immediately the relative magnitude of the two ionization processes and their interference. Clearly, this enables one to control the magnitude of all  $|m\lambda_n - n\lambda_m|$  minima of the distribution. The relative phase of the two beam components determines the orientation of these minima (and the whole distribution) within the polarization plane. A change in the phase  $\Phi$  rotates the electric field of the biharmonic field by an angle between zero and  $2\pi/|m\lambda_n - n\lambda_m|$ . The electric-field rotation is subsequently projected into the photoelectron distribution, with the dominant emission direction following the maxima of the electric field.

This control of circular dichroism in biharmonic ionization is shown in Fig. 2, where the photoelectron angular distributions are displayed for biharmonic ionization of helium by

counterrotating circularly polarized biharmonic beams with energies of 14.3 and 28.6 eV. All distributions were calculated within the lowest-order perturbation theory and using the independent particle approximation; see [35,36] for a detailed description. This example follows recent experiments on the ionization of helium atoms by a beam consisting of a fundamental frequency and its second harmonic [30] as observed at the Free Electron laser Radiation for Multidisciplinary Investigations (FERMI) free-electron laser. While only linearly polarized biharmonic beams were used before [30], circularly polarized beams can be generated at the FERMI free-electron laser [9,11,28]. The left panel in Fig. 2 shows photoelectron angular distributions in the polarization plane for biharmonic ionization of neutral helium atoms by a circularly polarized beam that comprises counterrotating fundamental frequency ( $\omega = 14.3$  eV) with intensity  $I(\omega) = 10^{14}$  W/cm<sup>2</sup> and its second harmonic with intensity  $I(2\omega) = 3.3 \times 10^{10}$  W/cm<sup>2</sup>, with  $\Phi = \pi/3$  phase between the two components. The green dashed line refers to biharmonic ionization with a beam consisting of right-circularly polarized fundamental frequency and a left-circularly polarized second harmonic, while the solid black line represents the ionization distribution with the helicities of both field components reversed. The circular dichroism is given by the normalized difference of the ionization rates  $dW_{\lambda_m \lambda_n}^{nm}$  and  $dW_{-\lambda_m -\lambda_n}^{nm}$ , while all other parameters remain unchanged [see Eq. (5)]. As seen directly from these distributions or, alternatively, from the color-coded plot of circular dichroism (ring around the distributions), the dichroism parameter is very low. To increase the circular dichroism, the intensity of the second harmonic must be increased. If the intensity is increased to  $I(2\omega) = 10^{12}$  W/cm<sup>2</sup>, the minima of the photoelectron angular distributions go to zero, and hence, a strong circular dichroism is expected. The corresponding distributions and circular dichroism are shown in the middle plot in Fig. 2. Furthermore, the relative phase between the two beam components can be increased to an optimal value of  $\Phi = 11\pi/15$ , for which the minima coincide with the maxima in photoelectron angular distribution due to the ionization by opposite helicities. With the optimal phase between the beam components, the maximum possible circular dichroism can be detected, as shown in the right plot in Fig. 2.

Circular dichroism can be readily controlled for the photoelectron angular distribution of biharmonic ionization of *s* electrons of any atom. The possibility to control the dichroism arises from the angular momentum properties associated with the process and the fact that biharmonic ionization is determined by just two ionization pathways. Moreover, since the flux and phase difference of the two components of the incident beam effectively modify the conditions of the ionization process, the control of circular dichroism can also be achieved for any (fundamental) frequency. This is shown in Fig. 3 for biharmonic ionization of helium by a circularly polarized beam that consists of circularly polarized components with fundamental frequency  $\omega$  and its second harmonic. Figure 3 shows the two experimental parameters, the flux ratio  $\mu$  (top) and the phase difference  $\Phi$  between the two beam components (bottom) which are necessary to achieve maximum circular dichroism in the photoelectron angular distribution. The results presented in Fig. 3 lead to maximum circular dichroism for ionization of helium by both co- and counter-

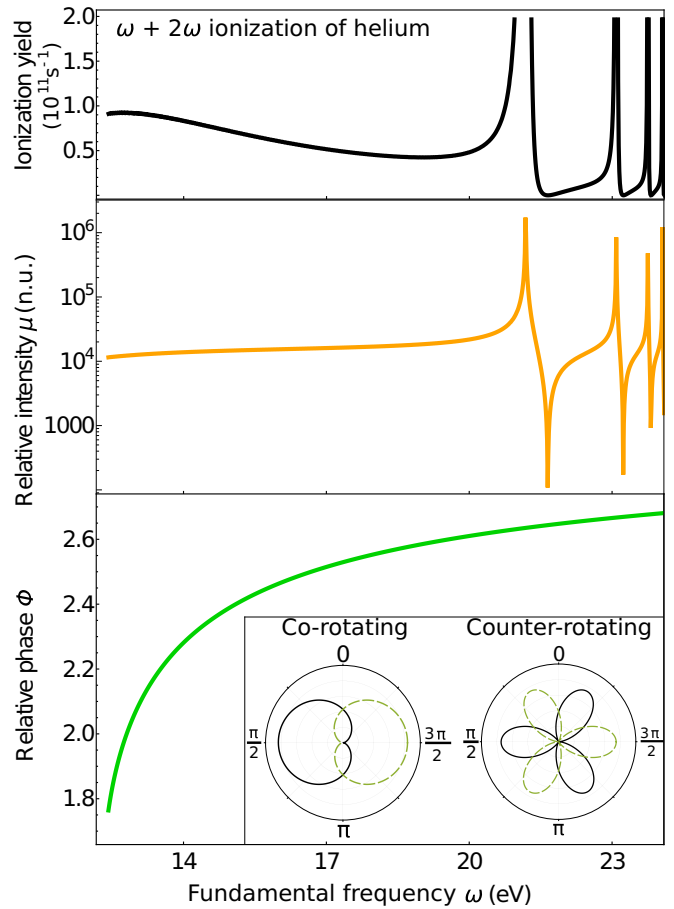


FIG. 3. Biharmonic ionization of neutral helium by a counterrotating circularly polarized beam consisting of a fundamental frequency  $\omega$  and its second harmonic. The total ionization yield (top), relative flux in natural units (middle), and phase (bottom) of the two biharmonic beam components are calculated as a function of the fundamental frequency in order to obtain the maximum circular dichroism. The inset in the bottom panel shows the photoelectron angular distributions in the polarization plane for biharmonic ionization of helium by a beam with co- and counterrotating components which are obtained by choosing any pair of  $\mu$  and  $\Phi$  at given energy  $\omega$ .

tating components of the incident beam (see the inset for the corresponding distributions). Apparently, the energy dependence of the values of these two experimental parameters, which lead to the maximum dichroism, closely follows the atomic parameters that determine the ionization process. The flux ratio varies slowly (with increasing photon energy) from the ionization threshold up to a photon energy which triggers the  $1s^2 \rightarrow 1s2p$  resonant transition. Near this resonance energy, the two-photon ionization cross section increases rapidly, which needs to be compensated by reducing the intensity of the fundamental frequency component of the beam. If the incident photon energy is further increased, the Cooper minimum in two-photon ionization is approached [35–38]. At this energy, the cross section of the two-photon ionization reaches its local minimum, which has to be balanced by an increase in the intensity of the fundamental beam component. This demand for varying the intensity ratio  $\mu$  repeats at higher photon energies, which are near  $1s^2 \rightarrow 1snp$

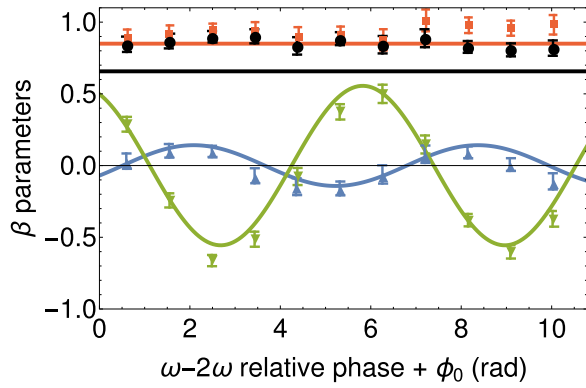


FIG. 4.  $\beta$  parameters as a function of  $\Phi + \phi_0$ . The markers represent  $\beta$  parameters extracted from Ref. [30]. Curves represent the  $\beta$  parameters as calculated in this work. The difference in parameters  $\beta_1 - 2\beta_3/3$  is represented by the blue curve and triangles,  $\beta_2$  is represented by the black curve and circles,  $\beta_3$  is represented by the green curve and inverted triangles, and  $\beta_4$  is represented by the red curve and squares.

resonant transitions. The phase difference between the two beam components, which leads to the maximum circular dichroism in the photoelectron angular distribution of biharmonic ionization, has a less sensitive energy dependence and is not affected by intermediate resonances.

To benchmark our calculations for helium atoms, we performed a comparison with two experiments. In the first experiment [39] the photoelectron angular distribution is measured after a two-photon ionization of helium by linearly polarized light with energies between  $\omega = 20.3$  eV and  $\omega = 24.3$  eV. A comparison of angular distributions was presented in our previous paper [35]; therefore, we do not repeat it here and draw only the conclusion that the experimental results perfectly agree with our calculations. However, such a comparison checks only one of the channels in Eq. (4). To evaluate the validity of our theoretical approach for biharmonic  $\omega + 2\omega$  ionization, we compared our calculations with the experimentally obtained results for biharmonic ( $\omega + 2\omega$ ) ionization of helium by linearly polarized light [30].

The authors of Ref. [30] presented their photoelectron angular distributions in terms of asymmetry parameters  $\beta_l$  from the expansion  $dW = \frac{W}{4\pi} [1 + \sum_l \beta_l P_l(\cos\theta)]$  with Legendre polynomials  $P_l(\cos\theta)$ . A comparison of the asymmetry parameters for the ionization of the ground state of helium with a beam with the fundamental frequency  $\omega = 14.3$  eV and its second harmonic is presented in Fig. 4. The curves show the  $\beta$  parameters as calculated with our methodology, where blue triangle, black circle, green inverted triangle, and red square markers correspond to  $\beta_1 - 2\beta_3/3$ ,  $\beta_2$ ,  $\beta_3$ , and  $\beta_4$ , respectively. The values of the decoherence parameter  $h = 0.262$  and the phase offset  $\phi_0 = 5.07$  rad were used in accordance with Ref. [30]. See [30] for a further description of the experiment and the extracted parameters. The agreement between our calculations and the experimental data supports the validity of our theoretical approach for the ionization of helium (and generally closed-shell) atoms in the limits of the perturbation theory.

In conclusion, we showed that maximum circular dichroism in photoelectron angular distributions of general biharmonic ionization (simultaneous  $n$ - and  $m$ -photon ionizations) can always be achieved by the control of only two experimental parameters. Such control of circular dichroism can be obtained for biharmonic ionization of  $s$  electrons for any atom and any incident photon energy. The main motivation of this Letter was to stimulate experimental efforts at current free-electron laser facilities; however, the control scheme can also be achieved at lower energies with tabletop lasers. The control of circular dichroism could also be used as a tool for precise extraction of physical parameters such as transition amplitudes and photoelectron phases of multiphoton ionization processes [30], as a tool in electron spectroscopy [40–42], or even for analyzing the purity of the XUV beam polarization.

#### ACKNOWLEDGMENT

A.V.V. acknowledges financial support by the Government of the Russian Federation through the ITMO Fellowship and Professorship Program.

- 
- [1] S. Baier, A. N. Grum-Grzhimailo, and N. M. Kabachnik, *J. Phys. B* **27**, 3363 (1994).
- [2] N. A. Cherepkov, V. V. Kuznetsov, and V. A. Verbitskii, *J. Phys. B* **28**, 1221 (1995).
- [3] N. L. Manakov, M. V. Frolov, B. Borca, and A. F. Starace, *J. Phys. B* **36**, R49 (2003).
- [4] A. N. Grum-Grzhimailo and M. Meyer, *Eur. Phys. J. Special Topics* **169**, 43 (2009).
- [5] A. K. Kazansky, A. V. Grigorieva, and N. M. Kabachnik, *Phys. Rev. Lett.* **107**, 253002 (2011).
- [6] M. Meyer, D. Cubaynes, D. Glijer, J. Dardis, P. Hayden, P. Hough, V. Richardson, E. T. Kennedy, J. T. Costello, P. Radcliffe, S. Düsterer, A. Azima, W. B. Li, H. Redlin, J. Feldhaus, R. Taïeb, A. Maquet, A. N. Grum-Grzhimailo, E. V. Gryzlova, and S. I. Strakhova, *Phys. Rev. Lett.* **101**, 193002 (2008).
- [7] S. Mondal, H. Fukuzawa, K. Motomura, T. Tachibana, K. Nagaya, T. Sakai, K. Matsunami, S. Yase, M. Yao, S. Wada, H. Hayashita, N. Saito, C. Callegari, K. C. Prince, P. O’Keeffe, P. Bolognesi, L. Avaldi, C. Miron, M. Nagasono, T. Togashi *et al.*, *J. Phys. B* **46**, 205601 (2013).
- [8] A. N. Grum-Grzhimailo and E. V. Gryzlova, *Phys. Rev. A* **89**, 043424 (2014).
- [9] T. Mazza, M. Ilchen, A. J. Rafipoor, C. Callegari, P. Finetti, O. Plekan, K. C. Prince, R. Richter, M. B. Danailov, A. Demidovich, G. De Ninno, C. Grazioli, R. Ivanov, N. Mahne, L. Raimondi, C. Svetina, L. Avaldi, P. Bolognesi, M. Coreno, P. O’Keeffe *et al.*, *Nat. Commun.* **5**, 3648 (2014).
- [10] T. Mazza, E. Gryzlova, A. Grum-Grzhimailo, A. Kazansky, N. Kabachnik, and M. Meyer, *J. Electron Spectrosc.* **204**, 313 (2015).
- [11] M. Ilchen *et al.*, *Phys. Rev. Lett.* **118**, 013002 (2017).

- [12] A. N. Grum-Grzhimailo, N. Douguet, M. Meyer, and K. Bartschat, *Phys. Rev. A* **100**, 033404 (2019).
- [13] R. Taïeb, V. Vénier, A. Maquet, N. L. Manakov, and S. I. Marmo, *Phys. Rev. A* **62**, 013402 (2000).
- [14] M. Fidirig and A. Cionga, *J. Phys. B* **35**, 821 (2002).
- [15] C. A. Mancuso, D. D. Hickstein, P. Grychtol, R. Knut, O. Kfir, X.-M. Tong, F. Dollar, D. Zusin, M. Gopalakrishnan, C. Gentry, E. Turgut, J. L. Ellis, M.-C. Chen, A. Fleischer, O. Cohen, H. C. Kapteyn, and M. M. Murnane, *Phys. Rev. A* **91**, 031402(R) (2015).
- [16] D. B. Milošević and W. Becker, *Phys. Rev. A* **93**, 063418 (2016).
- [17] C. A. Mancuso, D. D. Hickstein, K. M. Dorney, J. L. Ellis, E. Hasović, R. Knut, P. Grychtol, C. Gentry, M. Gopalakrishnan, D. Zusin, F. J. Dollar, X.-M. Tong, D. B. Milošević, W. Becker, H. C. Kapteyn, and M. M. Murnane, *Phys. Rev. A* **93**, 053406 (2016).
- [18] S. Odžak, E. Hasović, W. Becker, and D. B. Milošević, *J. Mod. Opt.* **64**, 971 (2017).
- [19] A. Gazibegović-Busuladžić, W. Becker, and D. B. Milošević, *Opt. Express* **26**, 12684 (2018).
- [20] J. L. Chaloupka, *J. Phys. B* **53**, 185601 (2020).
- [21] D. Pengel, S. Kerbstadt, D. Johannmeyer, L. Englert, T. Bayer, and M. Wollenhaupt, *Phys. Rev. Lett.* **118**, 053003 (2017).
- [22] S. Kerbstadt, K. Eickhoff, T. Bayer, and M. Wollenhaupt, *Adv. Phys.: X* **4**, 1672583 (2019).
- [23] G. S. J. Armstrong, D. D. A. Clarke, J. Benda, J. Wragg, A. C. Brown, and H. W. van der Hart, *Phys. Rev. A* **100**, 063416 (2019).
- [24] D. B. Milošević, W. Becker, and R. Kopold, *Phys. Rev. A* **61**, 063403 (2000).
- [25] A. N. Grum-Grzhimailo, E. V. Gryzlova, E. I. Staroselskaya, J. Venzke, and K. Bartschat, *Phys. Rev. A* **91**, 063418 (2015).
- [26] N. Douguet, A. N. Grum-Grzhimailo, E. V. Gryzlova, E. I. Staroselskaya, J. Venzke, and K. Bartschat, *Phys. Rev. A* **93**, 033402 (2016).
- [27] E. V. Gryzlova, M. M. Popova, A. N. Grum-Grzhimailo, E. I. Staroselskaya, N. Douguet, and K. Bartschat, *Phys. Rev. A* **100**, 063417 (2019).
- [28] K. C. Prince, E. Allaria, C. Callegari, R. Cucini, G. De Ninno, S. Di Mitri, B. Diviacco, E. Ferrari, P. Finetti, D. Gauthier, L. Giannessi, N. Mahne, G. Penco, O. Plekan, L. Raimondi, P. Rebernik, E. Roussel, C. Svetina, M. Trovò, M. Zangrando *et al.*, *Nat. Photonics* **10**, 176 (2016).
- [29] L. Giannessi, E. Allaria, K. C. Prince, C. Callegari, G. Sansone, K. Ueda, T. Morishita, C. N. Liu, A. N. Grum-Grzhimailo, E. V. Gryzlova, N. Douguet, and K. Bartschat, *Sci. Rep.* **8**, 7774 (2018).
- [30] M. Di Fraia *et al.*, *Phys. Rev. Lett.* **123**, 213904 (2019).
- [31] N. Douguet, E. V. Gryzlova, E. I. Staroselskaya, K. Bartschat, and A. N. Grum-Grzhimailo, *Eur. Phys. J. D* **71**, 105 (2017).
- [32] E. V. Gryzlova, A. N. Grum-Grzhimailo, E. I. Staroselskaya, N. Douguet, and K. Bartschat, *Phys. Rev. A* **97**, 013420 (2018).
- [33] P. Lambropoulos, *Phys. Rev. Lett.* **29**, 453 (1972).
- [34] D. Milošević, *Atoms* **6**, 61 (2018).
- [35] J. Hofbrucker, A. V. Volotka, and S. Fritzsche, *Phys. Rev. Lett.* **121**, 053401 (2018).
- [36] J. Hofbrucker, A. V. Volotka, and S. Fritzsche, *Sci. Rep.* **10**, 3617 (2020).
- [37] J. Hofbrucker, A. V. Volotka, and S. Fritzsche, *Phys. Rev. A* **100**, 011401(R) (2019).
- [38] J. Hofbrucker, L. Eiri, A. V. Volotka, and S. Fritzsche, *Atoms* **8**, 54 (2020).
- [39] R. Ma, K. Motomura, K. L. Ishikawa, S. Mondal, H. Fukuzawa, A. Yamada, K. Ueda, K. Nagaya, S. Yase, Y. Mizoguchi, M. Yao, A. Rouze, A. Hundermark, M. J. J. Vrakking, P. Johnsson, M. Nagasono, K. Tono, T. Togashi, Y. Senba, H. Ohashi *et al.*, *J. Phys. B* **46**, 164018 (2013).
- [40] M. Wollenhaupt, V. Engel, and T. Baumert, *Annu. Rev. Phys. Chem.* **56**, 25 (2005).
- [41] M. Wollenhaupt and T. Baumert, *Faraday Discuss.* **153**, 9 (2011).
- [42] S. Skruszewicz, J. Tiggesbäumker, K.-H. Meiwes-Broer, M. Arbeiter, T. Fennel, and D. Bauer, *Phys. Rev. Lett.* **115**, 043001 (2015).